Mechanisms of Ligand Association in Complexes of the Type $RML_3^+X^-$ (M = Ni, Pd, Pt). II. The Mechanisms of the Reactions $HML_3^+ + L \rightleftharpoons HML_4^+$ ($L = P(C_2H_5)_3$)

A. D. English,* P. Meakin,* and J. P. Jesson*

Contribution No. 2262 from the Central Research and Development Department, Experimental Station, E.I. du Pont de Nemours and Company, Wilmington, Delaware 19898. *Received April 18, 1975*

Abstract: The reaction $HML_3^+ + L \rightleftharpoons HML_4^+$ (M = Ni, Pd, Pt; L = $P(C_2H_5)_3$) has been studied in detail using $^{31}P\{^1H\}$ and ^1H NMR. The behavior of the NMR line shapes has been analyzed using general computer programs which include both inter- and intramolecular exchange effects. In addition to the k_1 and k_{-1} processes, rate processes corresponding to intramolecular rearrangement in both HML_3^+ and HML_4^+ species have been quantitatively analyzed. Detailed mechanistic information, such as the mode of ligand attack and the site occupied by the attacking ligand in the five-coordinate intermediate, has been developed. Direct spectroscopic evidence is presented for the five-coordinate intermediate for all three metals; the equilibrium lies to the right for Ni and very far to the left for Pt (acetone solution, −90 to +60°). The broad mechanistic details are essentially the same for all three metals: an HML_3^+ complex of C_{2v} symmetry undergoes association with a free ligand molecule to give an HML_4^+ intermediate of C_{3v} symmetry (strongly distorted trigonal bipyramidal). The HML_4^+ species, in the case of Pt, is of such low concentration over the temperature range −90 to +60° that its presence cannot be detected by direct spectroscopic techniques; very low temperature (−140°) NMR studies allow $HPtL_4^+$ to be observed directly; the studies in the −90° to +30° range show unambiguously that the attacking ligand ends in a position in $HPtL_4^+$ symmetry equivalent with the two trans ligands in $HPtL_3^+$ (i.e., in what would be the equatorial plane of the "trigonal bipyramid"). For Pt, the ligand dissociation from HML_4^+ (k_{-1}) is rapid relative to the rate of intramolecular rearrangement in HML_4^+ (k_m), i.e., $k_{-1} \gg k_m$, for Pd $k_{-1} \approx 10^2 k_m$, and for Ni $k_{-1} \ll k_m$.

In a preliminary communication,[1] qualitative analyses of NMR line shapes for the hydride region ^1H spectra and $^{31}P\{^1H\}$ spectra for $HNi[P(C_2H_5)_3]_3^+$, $HPd[P(C_2H_5)_3]_3^+$, and $HPt[P(C_2H_5)_3]_3^+$ were presented both as a function of temperature and as a function of added ligand concentration. It was concluded that ligand dissociation is much faster than intramolecular rearrangement in the five-coordinate intermediate $HPtL_4^+$. For the palladium analogue, both intermolecular ligand exchange and intramolecular rearrangement contribute to the NMR line shapes with the intermolecular exchange being the faster process throughout the temperature range (−90° to +60° in acetone). For $HNi[P(C_2H_5)_3]_4^+$ intramolecular exchange is faster than ligand dissociation. In this case, there was also evidence for intramolecular exchange in the four-coordinate complex. It was observed that the intermolecular exchange processes were accelerated by added ligand for all three cations in accord with eq 1.

$$HML_3^+ + L \underset{k_{-1}}{\overset{k_1}{\rightleftharpoons}} HML_4^+ \qquad (1)$$

In this paper, the NMR line shapes for the $HNiL_3^+$-L, $HPdL_3^+$-L, and $HPtL_3^+$-L systems in acetone are quantitatively analyzed as a function of ligand concentration, complex concentration, and temperature. Four separate rate processes are considered, k_1, k_{-1}, k_m (the rate of intramolecular rearrangement in HML_4^+), and k_m' (the rate of intramolecular rearrangement in HML_3^+). In the case of Ni, k_{-1}, k_m, and k_m' can be determined over certain temperature ranges, the k_m' process having been included explicitly. The $HNiL_3^+$ system is complex and some ambiguity remains in the interpretation of the spectra under some conditions. For Pd and Pt, the process corresponding to k_m' does not occur at an appreciable rate.

The line shape calculations and group theoretical analysis allow one to obtain detailed mechanistic information concerning the mode of ligand attack and the site occupied by the ligand in the five-coordinate intermediate. Competing rate processes are included in the calculations with the proper weighting leading to quantitative estimates of the ratios of rates such as k_{-1}/k_m.

The overall analysis relies heavily on the mathematical techniques developed in the preceding paper.[2] The calculations in the previous paper were illustrated using the $HPd[P(C_2H_5)_3]_3^+$-$P(C_2H_5)_3$ system. In the present paper, mathematical discussion has been kept to a minimum to facilitate a clear description of the experimental results and chemical conclusions.

Experimental Section

The complexes $HM[P(C_2H_5)_3]_3^+B(C_6H_5)_4^-$ (M = Ni, Pd, Pt) were prepared by methods developed by Dr. R. A. Schunn of this laboratory.[3]

NMR samples were prepared in acetone, or acetone-d_6, in a nitrogen atmosphere. The $^{31}P\{^1H\}$ NMR spectra were obtained at 36.43 MHz in the Fourier mode on a Bruker HFX-90 spectrometer with a Digilab FTS-NMR 3 data system and pulser. Ten-millimeter o.d. sample tubes were used with concentric 3-mm capillaries containing 1,2-dibromotetrafluoroethane as ^{19}F lock material or the capillary was omitted and acetone-d_6 was used as the solvent to provide a ^2H lock. In some experiments, chlorodifluoromethane was used as both the solvent and ^{19}F lock.

Hydride region ^1H NMR spectra were obtained at 90 MHz using the Bruker spectrometer in the time-shared mode with a Fabritek 1074 signal averager and at 100 MHz using a Varian HA100 spectrometer. Temperatures were measured for the Bruker HFX-90 using a copper-constantan thermocouple located just beneath the spinning NMR tube and were calibrated using a similar thermocouple held coaxially in a spinning NMR tube partially filled with solvent.

Mechanistic Considerations

A. Concerted Processes. In the previous paper, we have shown[2] that, for a planar HML_3^+ complex reacting with free ligand L in a concerted process, there are only six ways in which the arrangement of phosphorus nuclei before reaction can be related to their arrangement after exchange. Any postulated concerted mechanism must correspond to one or other of the six sets (or to a linear combination) so that it is possible to exclude certain mechanisms unambigu-

ously even though there are an infinite number of physical paths corresponding to each set. The six types of exchange are described below with an example of one possible physical mechanism for each set; in these examples, the numbering subscripts are removed from the ligands which are scrambled.

Sets I and II

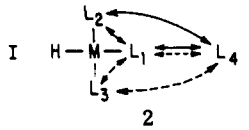

2

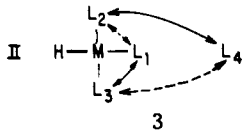

3

The two-headed arrows imply microscopic reversibility; the dotted and solid lines indicate processes which are equally probable by symmetry. Sets I and II are similar in that they are the only sets which scramble all four phosphorus ligands; the differences between sets I and II are subtle and have been described in the preceding publication.[2] A simple physical mechanism which scrambles all ligands, but does not correspond exclusively to I or II, is

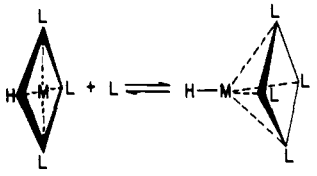

4

(ligand attack leading to a tetragonal pyramid with the hydride ligand in the apical position).

Set III

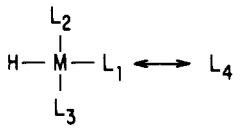

5

A possible physical mechanism, with L_4 attacking along the pseudo-C_4 axis of HML_3^+, is:

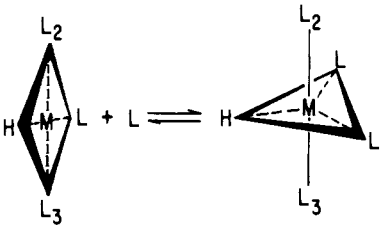

6

with L_2 and L_3 remaining equivalent and never scrambling with free ligand and with L_1 and L_4 scrambled.

Set IV

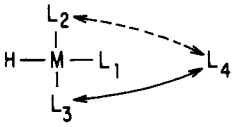

7

A possible physical mechanism, with L_4 attacking along the pseudo-C_4 axis of the HML_3^+ ion, is shown (**8**). L_1 remains unique and there is an equal probability of L_2, L_3, or L_4 dissociating in the reverse step, i.e., L_2, L_3, and L_4 are scrambled. This is shown to be the actual mechanism

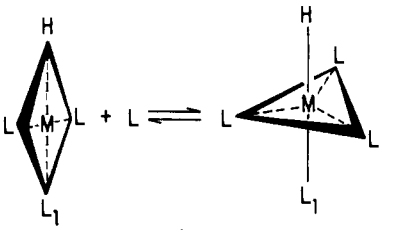

8

for the complexes discussed in this paper, neglecting for the moment intramolecular processes (vide infra), and corresponds to the linear combination (IV + E); since the identity permutation does not contribute, the line shape effects are the same as those for IV alone.

Set V

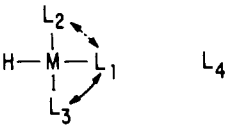

9

This could be ligand catalyzed or a simple intramolecular process, without participation of free ligand, a process (possibly solvent catalyzed) which is shown to occur in $HNiL_3^+$ and is assumed to involve interconversion between the stable "planar" form and a "tetrahedral" transition state or intermediate (configuration **10**).

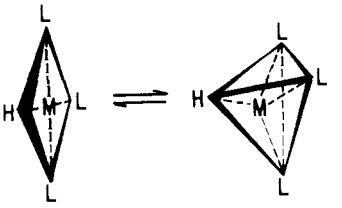

10

Set VI ≡ E

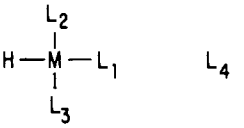

11

This could, of course, correspond to no chemical interaction with the free ligand. Another possibility is the process

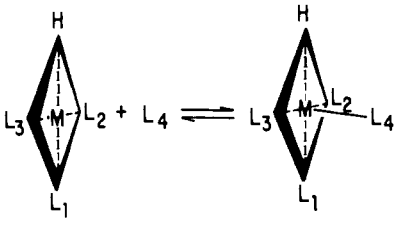

12

which corresponds to the formation of a distorted square pyramidal complex with L_4 in the apical position; since L_4 never becomes equivalent to L_1, L_2, or L_3, it must always be the ligand which dissociates. There is then no scrambling of the ligands and the labeling is the same before and after exchange. It is assumed that the concentration of the five-coordinate intermediate is vanishingly small.

B. Multistep Processes. It is shown below that, to the degree that the $HML_3^+ + L$ process can be considered to be concerted, it corresponds to sets E + IV. Detailed analyses of the NMR line shapes reveal that, in certain cases, one or two other rate processes must be considered as competing with the ligand association ↔ dissociation reaction. These

Table I. NMR Data for $HM[P(C_2H_5)]_3^+$ Compounds[a,b]

	^1H hydride spectrum					^{31}P $^1H\}$ spectrum					
	J_{HB}	J_{HA}	J_{HX}	δ_H	T, °C	J_{AB}	J_{XA}	J_{XB}	δ_A	δ_B	T, °C
Ni	±69	∓102		12.39	−73	25			−16.8	−15.1	−90
Pd	~0	182		7.80	−50	31			−20.6	−10.6	28
Pt	17.5	157	819	6.04	−50	20	±2057	±2510	−16.6	13.4	0

[a] All samples were dissolved in acetone-d_6. Coupling values are given in hertz. Chemical shifts are given in parts per million: ^1H is referred to TMS, ^{31}P is referred to 85% H_3PO_4. [b] Labeling as in configuration **14**.

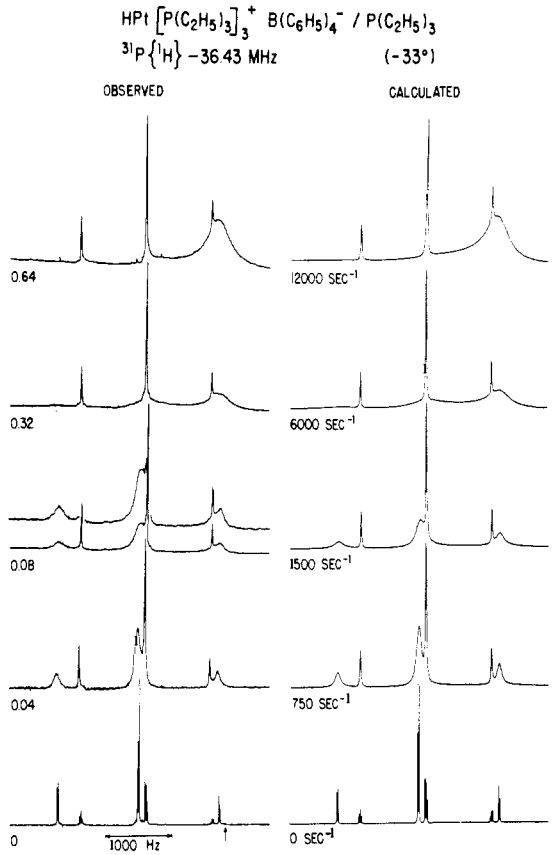

Figure 1. The 36.43-MHz Fourier mode proton noise decoupled ^{31}P NMR spectrum for a 0.17 *M* solution of $HPt[P(C_2H_5)_3]_3^+B(C_6H_5)_4^-$ in acetone as a function of added ligand concentration at −33°. The numbers beneath the observed spectra indicate the added ligand concentration (mole liter^{-1}) and the arrow indicates the resonance frequency of the free ligand. The numbers beneath the calculated spectra are $[1/\tau_{HML_3^+}]$.

are intramolecular rearrangement in the HML_4^+ intermediate and in the HML_3^+ starting material. In the previous paper,[2] we have shown that the competing intramolecular rearrangement in HML_4^+ can be taken into account by using a linear combination of the basic sets I-VI, provided the HML_4^+ concentration is small and its preexchange lifetime is short. The physical process:

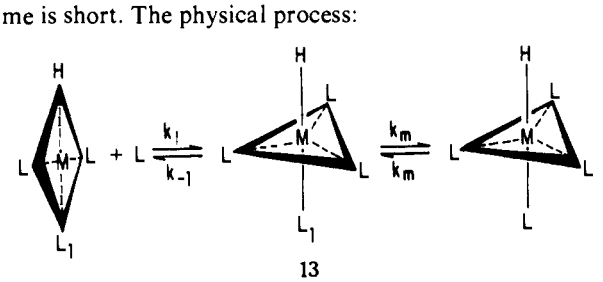

13

(in the first step L_1 remains unique, in the second step intramolecular rearrangement takes place in HML_4^+ at a rate k_m, scrambling L_1 with the equatorial ligands) can be represented by the linear combination:

$$(1 - C)(E + IV) + (C/3)(I + II + III + V) \quad (2)$$

where

$$C = \tfrac{3}{4}\left[\frac{4k_m/3k_{-1}}{1 + 4k_m/3k_{-1}}\right] \quad (3)$$

Line Shape Analysis for $HPt[P(C_2H_5)_3]_3^+B(C_6H_5)_4^-$–$P(C_2H_5)_3$–Acetone

A. $^{31}P\{^1H\}$ NMR Spectra. The $^{31}P\{^1H\}$ NMR spectrum for a solution of $HPt[P(C_2H_5)_3]_3^+B(C_6H_5)_4^-$ in acetone consists of an AB_2 pattern (66.3% of Pt with zero spin) together with an AB_2X pattern (33.7% of ^{195}Pt with spin ½). NMR parameters are given in Table I. The spectra are essentially temperature independent over the range −95° to +60° in the absence of added ligand. The AB_2–AB_2X pattern is consistent with the structure

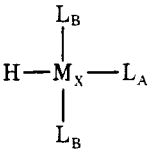

14

The left-hand side of Figure 1 shows the Fourier mode 36.43-MHz $^{31}P\{^1H\}$ NMR spectra for a 0.17 *M* solution of $HPt[P(C_2H_5)_3]_3^+B(C_6H_5)_4^-$ as a function of added ligand concentration at a constant temperature of −33°. The calculated spectra on the right-hand side of the figure were obtained by first fitting the NMR spectrum in the absence of added ligand. The ligand exchange rate for 0.04 mol l.$^{-1}$ of added ligand was then obtained by fitting the NMR spectrum using a $(3 \times HML_3^+)/L$ model (to include the ^{195}Pt satellite resonances) with basic permutational set IV, (E + IV) (**7**). The other calculated spectra were obtained by decreasing the preexchange lifetime for HML_3^+ and increasing $[L]/[HML_3^+]$ in proportion to the added ligand concentration. No attempt was made to vary the exchange rates to fit the observed spectra. The good agreement between the calculated and observed spectra in Figure 1 indicates that

$$1/\tau_{HML_3^+} \propto [L]^{1.0} \quad (4)$$

establishing the associative nature of the exchange process.

A similar set of experiments in which the $HPtL_3^+$ concentration is varied keeping [L] fixed at constant temperature is shown in Figure 2. These spectra were obtained from a solution of 25 μl of $P(C_2H_5)_3$ in 2 cm^3 of acetone (~0.085 *M* in $P(C_2H_5)_3$) to which increments of $HPt[P(C_2H_5)_3]_3^+B(C_6H_5)_4^-$ were added corresponding to successive totals of 30, 60, 120, and 240 mg of the complex. For an associative process such as **8**, the preexchange lifetime $\tau_{HML_3^+}$ should be independent of $[HML_3^+]$. However, Figure 2 shows that the exchange rate with respect to HML_3^+ $(1/\tau_{HML_3^+})$ becomes slower as the HML_3^+ concentration is increased. Several factors could contribute to this effect including: (A) reduction in the L concentration

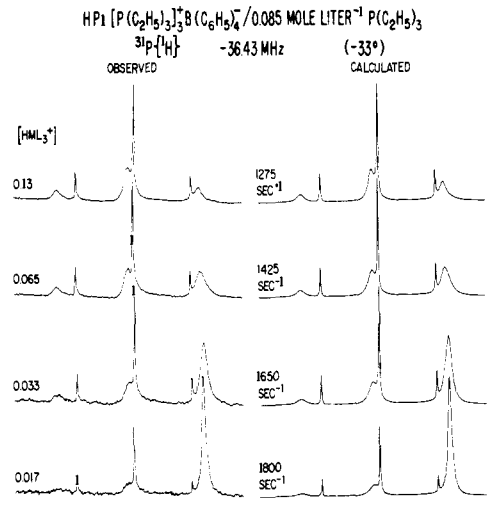

Figure 2. The 36.43-MHz $^{31}P\{^1H\}$ for several solutions of $HPt[P(C_2H_5)_3]_3^+B(C_6H_5)_4^-$ in a 0.085 *M* solution of $P(C_2H_5)_3$ in acetone-d_6 as a function of $HPt[P(C_2H_5)_3]_3^+B(C_6H_5)_4^-$ concentration at −33°. The exchange rates are the rates at which HML_3^+ undergoes ligand association to form HML_4^+.

because of the increase in volume of the solution on adding HML_3^+, (B) reduction in the L concentration due to formation of HML_4^+, (C) a change in the reaction rate resulting from a change in the "solvent" as the HML_3^+ concentration is increased, (D) partial decomposition of $P(C_2H_5)_3$ by a minor impurity in the HML_3^+ complex, (E) formation of a small amount of a dimeric Pt species. On increasing the HML_3^+ concentration from ~0.017 *M* (30 mg of HML_3^+) to ~0.13 *M* (240 mg of HML_3^+), the exchange rate decreased by ~30%. The change in total volume can account for no more than 5% of this. Formation of HML_4^+ cannot be an important factor since a sufficiently large value for the equilibrium constant $[HML_4^+]/[HML_3^+][L]$ would imply that HML_4^+ should be directly detectable by NMR under conditions of large L and HML_3^+ concentrations at low temperatures. We can obtain no evidence for HML_4^+ under these conditions in acetone, but resonances assigned to HML_4^+ are observed in HML_3^+-L solutions in chlorodifluoromethane at very low temperatures (vide infra). The most likely explanation is that changing the HML_3^+ concentration from 0.017 to 0.13 *M* alters the nature of the reaction medium sufficiently to change the rate constant by 30%. Repeating the experiment at a lower temperature (−73°), using a larger [L] (0.225 mol $l.^{-1}$) gave a similar but smaller (20%) decrease in exchange rate on raising $[HML_3^+]$ from 0.017 to 0.13 mol $l.^{-1}$.

Direct evidence for the HML_4^+ intermediate was found in concentrated HML_3^+-L solutions in $CHClF_2$ at very low temperatures. The $^{31}P\{^1H\}$ spectrum of a solution containing 0.20 mol $l.^{-1}$ of $P(C_2H_5)_3$ and 0.26 mol $l.^{-1}$ of $HPt[P(C_2H_5)_3]_3^+B(C_6H_5)_4^-$ in $CHClF_2$ at −131° shows resonances assigned to HML_4^+ and L as well as HML_3^+ (Figure 3). The $^{31}P\{^1H\}$ NMR spectrum for the HML_4^+ cation consists of an AB_3 pattern together with an AB_3X pattern (^{195}Pt, $I = \frac{1}{2}$). This spectrum is consistent with a structure such as **15** having C_{3v} symmetry, rigid on the NMR time scale. The NMR parameters are given in Table II. The $^{31}P\{^1H\}$ spectrum of a solution containing 0.45 mol

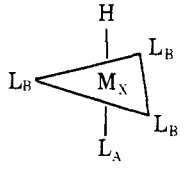

15

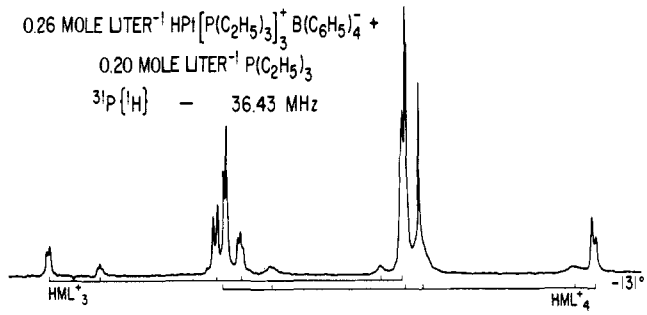

Figure 3. $^{31}P\{^1H\}$ NMR spectrum of a solution containing $HPt[P(C_2H_5)_3]_3^+B(C_2H_5)_4^-$ (0.26 mol $l.^{-1}$) and $P(C_2H_5)_3$ (0.20 mol $l.^{-1}$) in $CHClF_2$ at −131°C. AB_2, AB_2X, AB_3, and AB_3X patterns are observed.

Table II. NMR Data for $HM[P(C_2H_5)_3]_4^+$ Compounds[a–c]

M	δ_A[d]	δ_B[d]	δ_H	J_{AB}	J_{XA}	J_{XB}	*T*, °C
Pt	0.4	− 3.0		31	±2125	±2730	−137
Pd	−23.4[e]	−23.4[e]					−160
Ni	−25.4	−29.7	19.5				−160

[a] In $CHClF_2$. [b] Labeling as in configuration 15. [c] Coupling constants in hertz. [d] Chemical shifts in parts per million upfield from $P(C_2H_5)_3$. [e] Single, unresolved resonance.

$l.^{-1}$ of $P(C_2H_5)_3$ and 0.14 mol $l.^{-1}$ of $HPt[P(C_2H_5)_3]^+B(C_6H_5)_4^-$ in $CHClF_2$ at −137° shows resonances assigned to HML_4^+ and L. Under these conditions, the equilibrium is so far to the right of eq 1 that the HML_3^+ resonances cannot be observed. At −114° resonances assigned to HML_4^+, HML_3^+, and L can still be observed but the HML_4^+ resonances are weak, and at −102° HML_4^+ cannot be detected. The strong temperature dependence of the equilibrium constant for reaction 1 is not unexpected since the forward step

$$HML_3^+ + L \rightarrow HML_4^+$$

is only weakly temperature dependent (vide infra) while the reverse step

$$HML_4^+ \rightarrow HML_3^+ + L$$

is anticipated to be strongly temperature dependent (nonzero $\Delta H^\ddagger$ and small $\Delta S^\ddagger$). Assuming that the behavior in acetone is similar to that in chlorodifluoromethane (this assumption has been shown to be correct for $HPdL_3^+$-L at −80°C), $[HML_4^+]$ will decrease strongly with increasing temperature in HML_3^+-L solutions and the assumption that $[HML_4^+] \rightarrow 0$, which was used in the line shape analysis, is well justified, particularly at temperatures in the range −90° to +60°.

Figures 1 and 2 together with exchange rates at HML_3^+ and L concentrations not shown in these figures indicate that

$$1/\tau_{HML_3^+} \propto [L]^{1.0}[HML_3^+]^{-0.15} \approx [L][HML_3^+]^0 \text{ at } 33°$$

Figure 4 shows observed and calculated $^{31}P\{^1H\}$ NMR spectra for a 0.17 *M* solution of the $HPtL_3^+$ complex with 0.08 mol $l.^{-1}$ added ligand as a function of temperature. In this case, the exchange rate was varied to give the best visual fit between observed and calculated spectra. In comparing the observed and calculated spectra in Figures 1, 2, and 4, it should be noted that the experimental spectra are distorted by the audio filter used in the Fourier mode experiment (intensities are exponentially decreased from left to right in the spectra). To obtain a good fit between the calculated and observed spectra, it was necessary to decrease $T_2(HML_3^+)$ (increase the line width in the absence of ex-

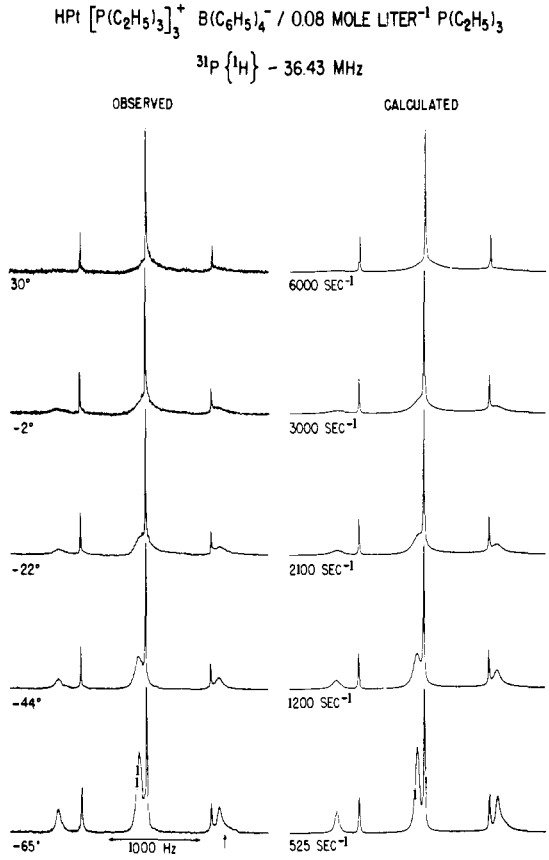

Figure 4. Fourier mode $^{31}P\{^1H\}$ NMR spectrum for an acetone solution of $HPt[P(C_2H_5)_3]_3^+B(C_6H_5)_4^-$ (0.17 *M*) and $P(C_2H_5)_3$ (0.08 *M*) as a function of temperature. The arrow indicates the resonance frequency of free ligand. The exchange rates given with the calculated spectra are the pseudo-first-order rate constants for the addition of L to $HPtL_3^+$ $[(\tau_{HPtL_3^+})^{-1}]$.

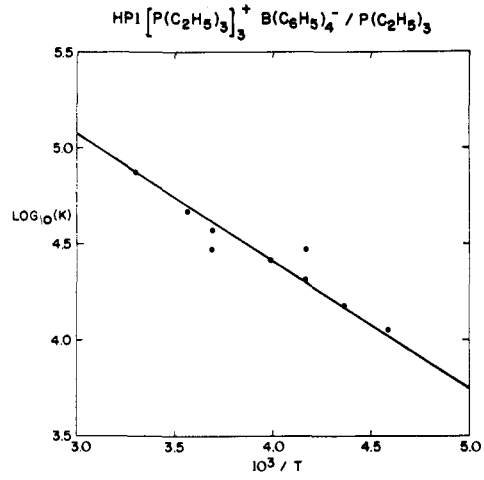

Figure 5. Arrhenius plot for kinetic data obtained from line shape analysis for 0.17 *M* $HPt[(C_2H_5)_3]_3^+$/0.08 *M* $P(C_2H_5)_3$. The exchange rates have been reduced to those for $P(C_2H_5)_3$ at unit activity.

change) from the value used to fit the slow exchange limit spectra. However, an almost constant $T_2(HML_3^+)$ could be used to fit all of the spectra shown in Figures 1, 2, and 4 except for the slow exchange limit. The presence of a small quantity of the five-coordinate intermediate could be responsible for this additional broadening.[2]

Figure 5 shows an Arrhenius plot for the kinetic data obtained from the line shape analysis shown in Figure 4, and other data obtained from fitting line shapes for 0.17 *M* $HPtL_3^+$/0.08 *M* L. $(\tau_{HPtL_3^+})^{-1}$/[L] is plotted against $1/T$.

Table III. Thermodynamic Data (L = PEt_3)

Process	$\Delta G^\ddagger$ (kcal mol^{-1})	$\Delta H^\ddagger$ (kcal mol^{-1})	$\Delta S^\ddagger$ (cal mol^{-1} deg^{-1})	Log *A*	E^a (kcal mol^{-1})	*T* (°K)
$L + HPtL_3^+ \rightarrow HPtL_4^+$	10.9	2.4	−28.5	7.0	3.0	298
$L + HPdL_3^+ \rightarrow HPdL_4^+$	10.2	1.9	−27.8	7.07	2.4	298
$HNiL_4^+ \rightarrow HNiL_3^+ + L$	9.5	9.7	1.0	13.3	10.1	200
$HNiL_3^+$ (intramolecular)	11.2	9.6	− 7.9	11.3	10.0	200
$HNiL_4^+$ (intramolecular)	5.6					126

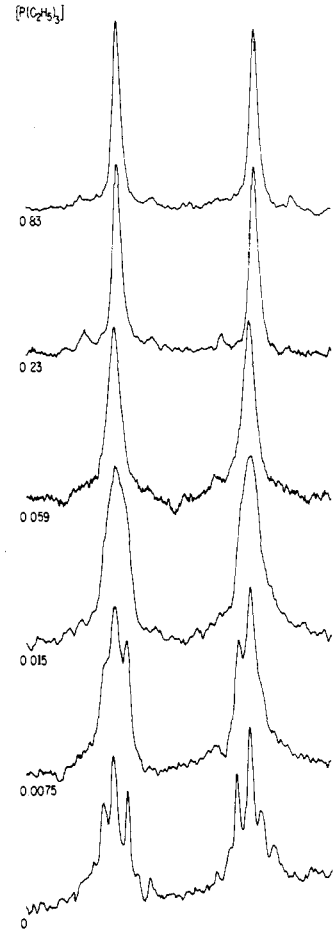

Figure 6. Hydride region ^1H NMR spectrum for a solution of $HPt[P(C_2H_5)_3]_3^+B(C_6H_5)_4^-$ in acetone-d_6 as a function of added ligand concentration (mole liter^{-1}) at −50°.

The straight line shown in Figure 5 corresponds to the rate expression.

$$k_1(T) = 10^{7.07}e^{-3030/RT}\ \text{l. mol}^{-1}\ \text{sec}^{-1}$$

A least-squares fit[4] using the Eyring equation gives the thermodynamic parameters shown in Table III. The large negative entropy of activation is consistent with an associative process.

B. Hydride Region ^1H NMR Spectra. The hydride region ^1H NMR spectrum of $HPt[P(C_2H_5)_3]_3^+B(C_6H_5)_4^-$-$P(C_2H_5)_3$ in acetone-d_6 is shown in Figure 6 as a function of added ligand concentration at constant temperature, and in Figure 7 as a function of temperature with fixed ligand concentration. NMR parameters are given in Table I. Only the central part of the spectrum corresponding to platinum

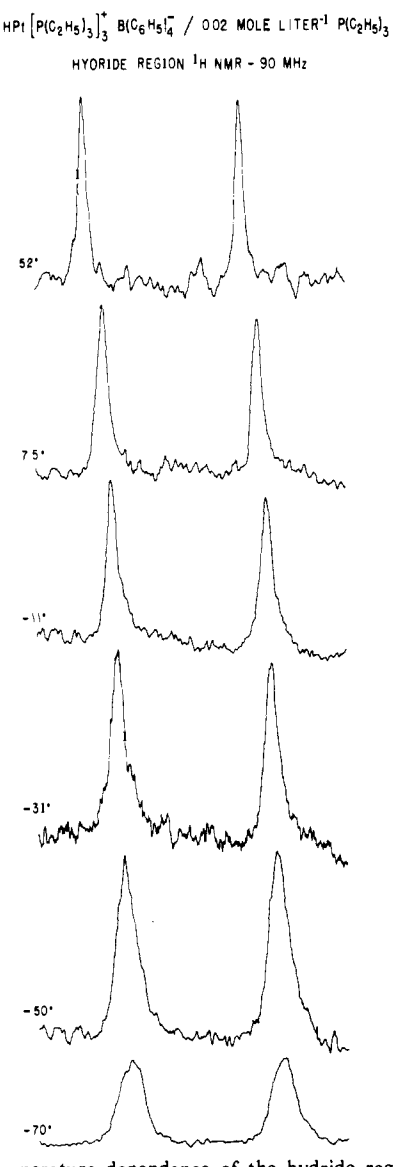

Figure 7. Temperature dependence of the hydride region ^1H NMR spectrum for an acetone solution of $HPt[P(C_2H_5)_3]_3^+B(C_6H_5)_4^-$ with 0.02 mol $l.^{-1}$ of added ligand.

isotopes with zero spin is shown. These spectra are not suitable for *quantitative* line shape analysis since they depend on ligand proton-phosphorus couplings as well as hydride proton-phosphorus couplings.[5] The spin system is too large for the line shape analysis to be tractable. Figure 8 shows the hydride region NMR spectrum for $HPt[P(C_2H_5)_3]_3^+$ calculated using an AB_2X model. The concentration of the five-coordinate intermediate is assumed to be vanishingly small and the calculations employed the linear combination (E + IV) (no mutual exchange in the HML_4^+ intermediate). The high resolution NMR parameters were $J_{AB} = -20$ Hz, $J_{AX} = 162.5$ Hz, $J_{BX} = -17.5$ Hz, and $\delta_B - \delta_A = 118$ Hz. The slow exchange limit spectrum calculated using these parameters is not in particularly good agreement with the observed slow exchange limit spectra; however, the observed spectra in Figures 6 and 7 are in qualitatively good agreement with the calculated spectra in Figure 8. Attempts to fit the observed spectra using linear combinations of other basic permutational sets gave poor agreement. The spectra shown in Figures 6 and 7 can be interpreted qualitatively in terms of an associative process which maintains the unique relationship between the hydride ligand and the trans phosphine ligand. Attempts to obtain *direct* evidence

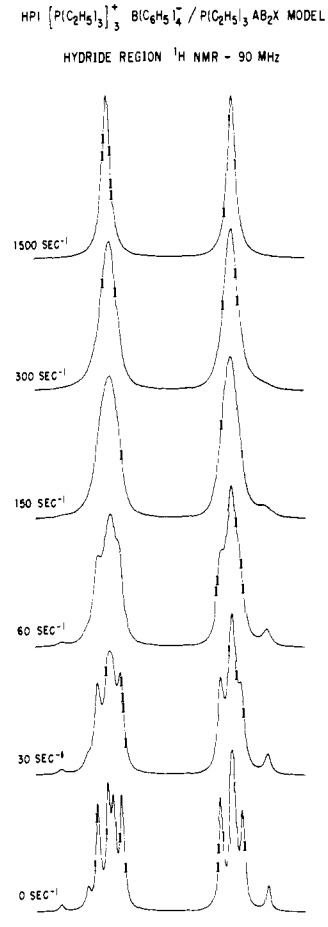

Figure 8. Simulation of the hydride region ^1H NMR spectrum for $HPt[P(C_2H_5)_3]_3^+B(C_6H_5)_4^-$ as a function of exchange rate using an AB_2X model. The exchange rate is the rate at which free ligand adds to the complex.

for the HML_4^+ intermediate, in acetone solutions of high ligand concentration, at both low temperatures (direct observation of the HML_4^+ resonances) and at high temperatures (observation of a shift of the hydride resonances) were not successful. The concentration of HML_4^+ must be low under all conditions so that use of the HML_3^+-L model, eliminating explicit inclusion of the HML_4^+ resonances in the line shape calculations, is again well justified.

Line Shape Analysis for $HPd[P(C_2H_5)_3]_3^+B(C_6H_5)_4^-$-$P(C_2H_5)_3$-Acetone

A. $^{31}P\{^1H\}$ NMR Spectra. The $^{31}P\{^1H\}$ NMR spectrum assigned to solutions of $HPd[P(C_2H_5)_3]_3^+B(C_6H_5)_4^-$ in acetone-d_6 is an AB_2 pattern (parameters are given in Table I). In the absence of added ligand, the spectra are temperature independent over the range −95° to +60°.

Figure 9 shows the temperature dependence of the $^{31}P\{^1H\}$ NMR spectrum for a solution of 0.17 mol $l.^{-1}$ of $HPd[P(C_2H_5)_3]_3^+B(C_6H_5)_4^-$/0.015 mol $l.^{-1}$ of $P(C_2H_5)_3$ in acetone-d_6 as a function of temperature. The calculated spectra on the right-hand side were obtained using an HML_3^+-L model with the linear combination of basic sets given in eq 2. The two rates given with the calculated spectra are the sums of the rates for the permutations in the linear combinations of sets (E + IV) and (I + II + III + V), respectively. The ratio k_m/k_{-1} for the five-coordinate intermediate can be obtained using eq 2 and 3. In those cases where the total rate for (E + IV) is much greater than that for I + II + III + V, eq 3 gives

$$\frac{k_m}{k_{-1}} = \frac{\text{rate(I + II + III + V)}}{\text{rate(E + IV)}}$$

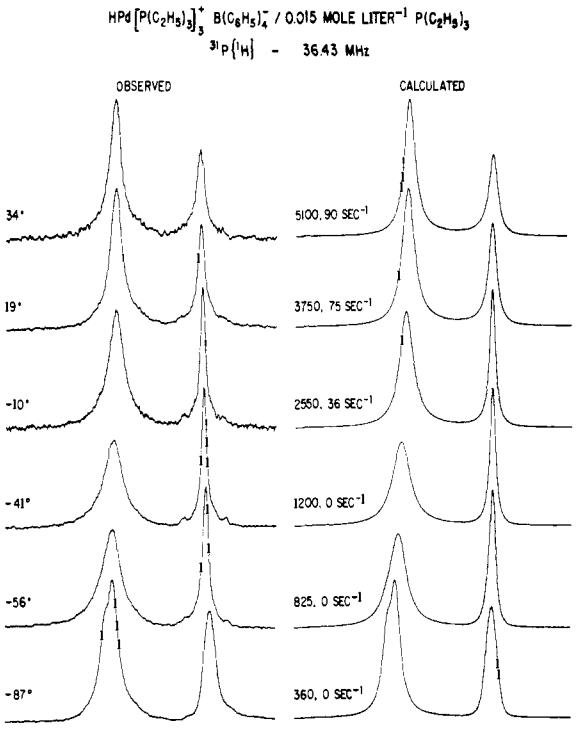

Figure 9. Temperature dependence of the $^{31}P\{^1H\}$ NMR spectra for a solution of 0.17 mol $l.^{-1}$ of $HPd[P(C_2H_5)_3]_3^+B(C_6H_5)_4^-$ and 0.015 mol $l.^{-1}$ of $P(C_2H_5)_3$ in acetone-d_6. The significance of the exchange rates given with the calculated spectra is described in the text.

Table IV. Estimates[a] of k_m/k_{-1} for $HPd[P(C_2H_5)_3]_4^+$

Solution A: 0.17 mol $l.^{-1}$ of HML_3/0.015 mol $l.^{-1}$ of L		Solution B: 0.13 mol $l.^{-1}$ of HML_3/0.58 mol $l.^{-1}$ of L	
k_m/k_{-1}	T	k_m/k_{-1}	T
~0	−41	0.0075	−91
0.014	−10	0.0084	−78
0.02	19	0.0118	−60
0.018	34	0.0103	−42
		0.0111	−23
		0.0126	− 5
		0.0150	22
		0.024	58

[a] Values for solution B are considered to be the most accurate.

leading to the results in the first column of Table IV. At temperatures below about −10°, the NMR line shapes are not sensitive to k_m/k_{-1}, but the observed spectra cannot be fitted unless k_m/k_{-1} is $\ll 1$. Figure 9 shows only that region of the spectrum near the HML_3^+ resonances since $[L]/[HML_3^+]$ is small. Even at very low temperatures (−90°), the free ligand resonance is very broad because of the exchange process, and cannot be seen in the spectrum. At higher temperatures, the free ligand resonance has coalesced with the HML_3^+ resonances.

Figure 10 shows the temperature dependence of the $^{31}P\{^1H\}$ NMR spectra for a solution of 0.13 mol $l.^{-1}$ of $HPd[P(C_2H_5)_3]_3^+B(C_6H_5)_4^-$/0.58 mol $l.^{-1}$ of $P(C_2H_5)_3$. The ratios of the rates of mutual exchange to dissociation in the HML_4^+ intermediate (k_m/k_{-1}) at a variety of temperatures are given in Table IV. The values obtained for (k_m/k_{-1}) in the two experiments corresponding to Figures 9 and 10 are considered to be in reasonably good agreement, with those from Figure 10 being the more accurate. These quantitative results confirm our earlier conclusions,[1] obtained from a qualitative examination of the $^{31}P\{^1H\}$ and hydride region ^1H NMR spectra, that the rate of ligand dissociation in $HPd[P(C_2H_5)_3]_4^+$ is greater than the rate of intramolec-

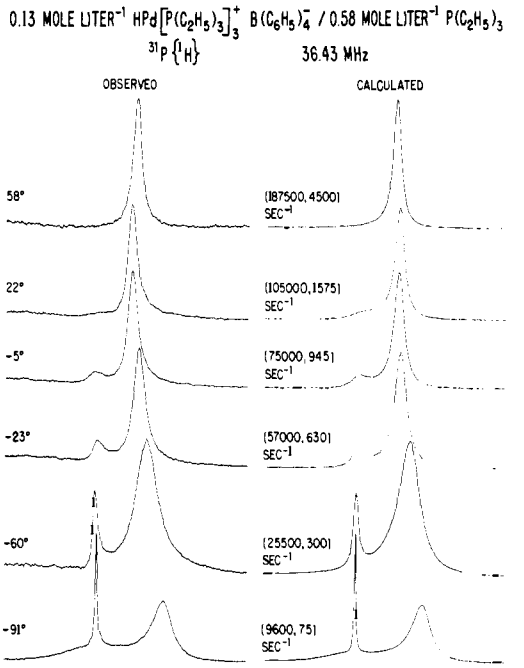

Figure 10. Temperature dependence of the $^{31}P\{^1H\}$ NMR spectrum for 0.13 mol $l.^{-1}$ of $HPd[P(C_2H_5)_3]_3^+B(C_6H_5)_4^-$ with 0.58 mol $l.^{-1}$ of $P(C_2H_5)_3$ in acetone-d_6. The two rates shown with the calculated spectra are the sums of the rates for the permutations in the linear combinations of basic sets (E + IV) and (I + II + III + V), respectively.

ular rearrangement at all temperatures in the range −90° to +35°. The small temperature dependence of (k_m/k_{-1}) indicates that both ligand dissociation and mutual exchange must have very similar activation energies. Since both k_m and k_{-1} should be *strongly* temperature dependent, we conclude that the HML_4^+ concentration must decrease rapidly with temperature (the forward and reverse rates of reaction **8** must be equal at all temperatures at equilibrium and the forward rate of reaction **8** is only weakly temperature dependent (Figures 9 and 10)).

A comparison of Figures 9 and 10 indicates that the ratios of $(1/\tau_{HML_3^+})$ values are smaller than the ratios of the free ligand concentrations. A similar effect was observed in the hydride region ^1H NMR spectra (vide infra). Again, the rather large ligand concentration used in the experiment corresponding to Figure 10 may have changed the solvent effect sufficiently to influence the rate constant for the reaction. Similar experiments have been carried out for a wide range of added ligand concentrations. They have not all been analyzed quantitatively, but they are all in qualitative agreement with an interpretation in terms of the reaction shown in **13** with $k_m \ll k_{-1}$ for $HPd[P(C_2H_5)_3]_4^+$. The model calculations shown in the preceding paper were used in these qualitative analyses.[2]

An Arrhenius plot for $(\tau_{HPdL_3^+})^{-1}/[L]$ constructed from the data in Figure 10 and other data from the same solution (0.13 *M* $HPdL_3^+$/0.58 *M* L) gives the rate expression

$$k_1(T) = 10^{7.07}e^{-2400/RT}\ l.\ mol^{-1}\ sec^{-1}$$

and a least-squares fit[4] using the Eyring equation gives the values in Table III.

As for the $HPtL_3^+$-L system, the entropy of activation is large and negative consistent with an associative process. The similarity in the magnitudes of the entropies of activation for the $HPtL_3^+$-L and the $HPdL_3^+$-L reaction (Table III) is consistent with both systems exchanging by the same mechanism.

The $^{31}P\{^1H\}$ NMR spectrum for a solution containing 0.11 mol $l.^{-1}$ of $P(C_2H_5)_3$ and 0.053 mol $l.^{-1}$ of

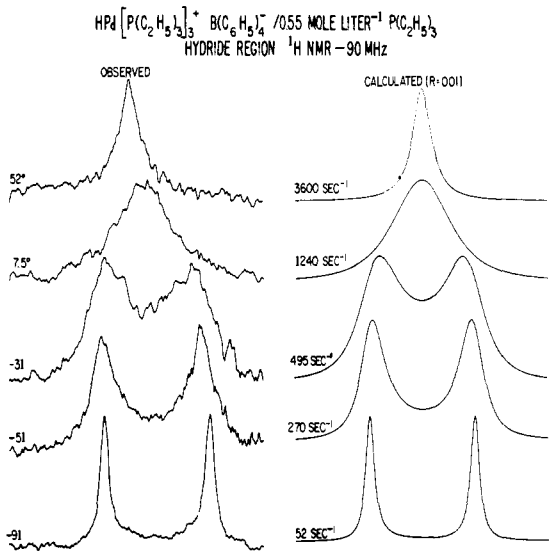

Figure 11. Temperature dependence of the hydride region ^1H spectrum of 0.16 mol $l.^{-1}$ of $HPd[P(C_2H_5)_3]_3^+B(C_6H_5)_4^-$ and 0.55 mol $l.^{-1}$ of $P(C_2H_5)_3$ in acetone-d_6. The exchange rates are for the linear combination (I + II + III + V) of basic sets. They do not correspond to the rate at which HML_3^+ adds L to form HML_4^+.

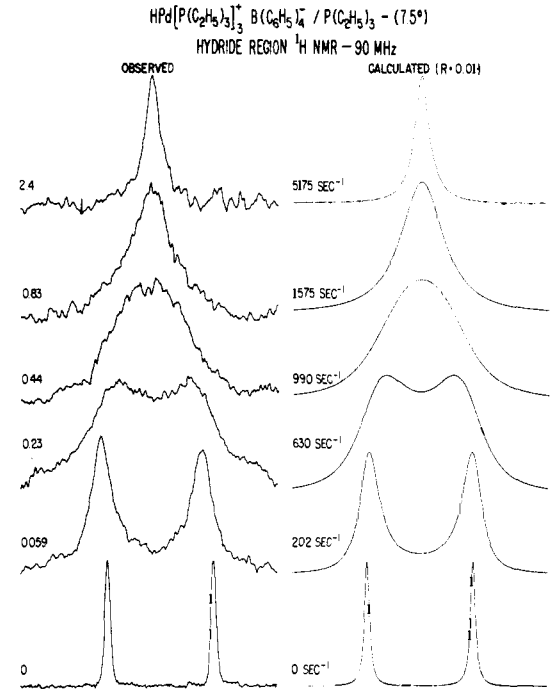

Figure 12. Observed and calculated hydride region ^1H NMR spectrum of a solution of $HPd[P(C_2H_5)_3]_3^+B(C_6H_5)_4^-$ (~0.15 mol $l.^{-1}$) as a function of added ligand concentration.

$HPd[P(C_2H_5)_3]_3^+B(C_6H_5)_4^-$ in chlorodifluoromethane contains resonances which can be assigned to HML_3^+, HML_4^+, and L at −160°. The HML_4^+ spectrum consists of a single unresolved resonance at −23.4 ppm upfield from internal $P(C_2H_5)_3$. On increasing the temperature, the intensity of the HML_4^+ spectrum decreases relative to that of the HML_3^+ spectrum; at a temperature of −148°, the HML_4^+ resonances are too weak to be observed. Since our analysis of the NMR line shapes for the HML_3^+-L system in acetone indicates that the HML_4^+ cation should be stereochemically rigid on the NMR time state at these low temperatures (vide supra), we conclude that the ^{31}P chemical shifts for the axial and equatorial ligands must be very close to each other. As was observed for the $HPtL_3^+$-$HPtL_4^+$-L system, the equilibrium constant is, as expected, strongly temperature dependent.

At high temperatures (−90° to −50°), the $^{31}P\{^1H\}$ NMR spectra for the $CHClF_2$ solution exhibit temperature dependent line shape behavior very similar to that shown in Figure 10. Hence, the spectra observed using $CHClF_2$ as solvent show that line shape analysis based on the assumption $[HML_4^+] \rightarrow 0$ is justified for the acetone solutions.

B. Hydride Region ^1H NMR Spectra. The hydride region ^1H NMR spectrum of a solution of $HPd[P(C_2H_5)_3]_3^+B(C_6H_5)_4^-$ consists of a doublet (data in Table I). This spectrum is consistent with the structure **14**. For a second-row transition metal complex of this type, a large trans H-P coupling (J_{HP_B} = 187.5 Hz) and small cis couplings ($J_{HP_A} \sim 0$ Hz) would be expected.

The hydride region ^1H NMR spectra were analyzed before the $^{31}P\{^1H\}$ spectra (vide supra). Since $J_{HP_A} \sim 0$, the NMR line shapes are almost completely insensitive to the rates of the permutations in (E + IV). (E + IV) exchanges the ligands L_A with free ligand; the main effect of this process on the hydride region ^1H NMR spectrum is to decouple the P_A spins, and since these couplings are very small in the slow exchange limit, (E + IV) has practically no effect on the spectrum. However, the effect of the permutations (E + IV) must be included in a quantitative analysis of the NMR line shapes when the rates of the permutations in (I + II + III + V) are nonzero. In analyzing the hydride region NMR spectra, the parameter C (eq 3) was set equal to 0.01 ($k_m/k_{-1} \approx 0.01$) since a *qualitative* analysis of the ^1H and $^{31}P\{^1H\}$ spectra indicated that $k_m \ll k_{-1}$. Fortuitously, this value turned out to be quite close to that obtained in the subsequent *quantitative* analysis of the $^{31}P\{^1H\}$ spectra. In all cases, the calculations were repeated with C set to 0.1 and all other parameters unchanged. The results obtained for C = 0.1 and 0.01 were almost indistinguishable, and any value for C ($C \ll 1$) could have been used in the calculations described below.

Figure 11 shows the temperature dependence for a solution containing 0.16 mol $l.^{-1}$ of $HPd[P(C_2H_5)_3]_3^+B(C_6H_5)_4^-$ and 0.55 mol $l.^{-1}$ of $P(C_2H_5)_3$ in acetone-d_6 as a function of temperature. The rates given with the calculated spectra on the right-hand side of the figure correspond to the sums of the rates of the nine permutations in (I + II + III + V). To obtain the spectra shown in Figure 12, successive increments of $P(C_2H_5)_3$ were added to a solution of 150 mg of $HPd[P(C_2H_5)_3]_3^+B(C_6H_5)_4^-$ in 1 cm^3 of acetone-d_6. Again, the rates given with the calculated spectra are for the linear combination (I + II + III + V) of basic permutational sets. It should be noted that the exchange rates given with Figure 12 are *not* directly proportional to the added ligand concentration. A 40-fold increase in [L] increases the exchange rate by a factor of 25. It should also be noted that these spectra were *not* analyzed using a simple two site, one spin approximation despite the simple appearance of the spectra.

We were unable to obtain any *direct* evidence for the HML_4^+ intermediate in either the hydride region proton or $^{31}P\{^1H\}$ NMR spectra even under conditions of large [L] and $[HML_3^+]$ at low temperatures (−90° in acetone-d_6). However, we believe that the indirect evidence in favor of such an intermediate is compelling. This belief is confirmed by the direct observation of the HML_4^+ cation in the $^{31}P\{^1H\}$ spectrum at low temperatures using $CHClF_2$ as solvent.

Analysis of the NMR Spectra for the $HNi[P(C_2H_5)_3]_3^+B(C_6H_5)_4^-$–$P(C_2H_5)_3$–Acetone System

A. $^{31}P\{^1H\}$ NMR Spectra. In the low temperature limit, the $^{31}P\{^1H\}$ NMR spectrum for a solution of

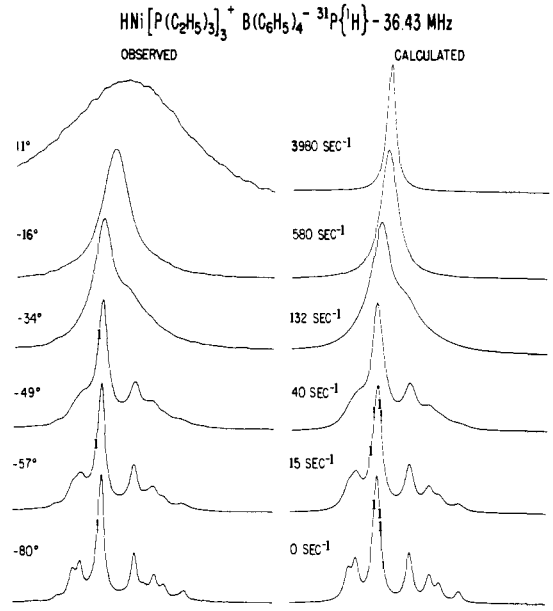

Figure 13. Observed and calculate temperature dependent $^{31}P\{^1H\}$ NMR spectra for a solution of $HNi[P(C_2H_5)_3]_3^+B(C_6H_5)_4^-$ in acetone-d_6. The calculated spectra were obtained using basic set V (mutual intramolecular exchange).

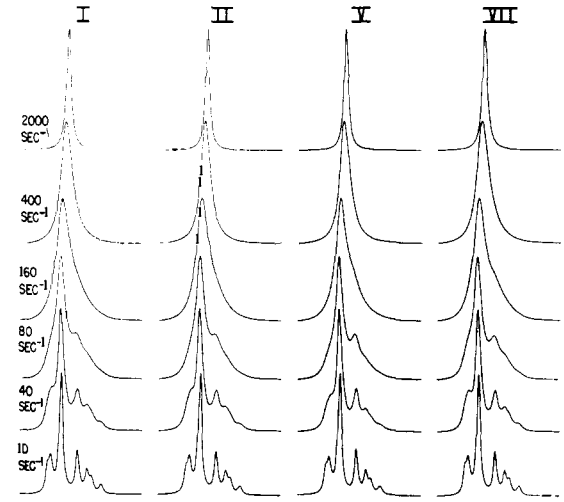

Figure 14. Calculated NMR line shapes for an HML_3^+-L system near the limit $[L]/[HML_3^+] \rightarrow 0$ as a function of exchange rate and mechanism (basic set). $[L]/[HML_3^+]$ was set to 0.00025, and the low temperature limit parameters for M = Ni were used. The column headings indicate the basic set used (VII represents the linear combination [I + II + III + IV + V + (VI = E)]).

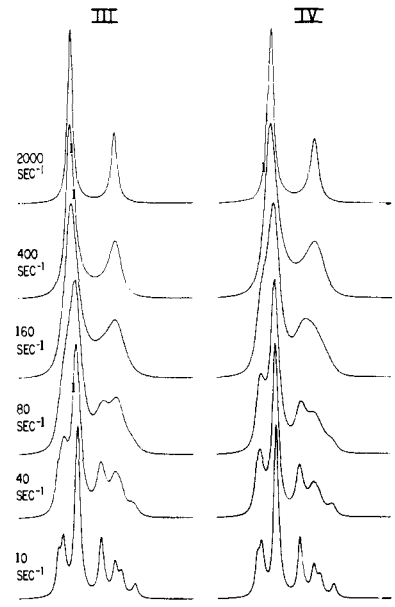

Figure 15. This figure is a continuation of Figure 14 for basic sets III and IV.

$HNi[P(C_2H_5)_3]_3^+B(C_6H_5)_4^-$ in acetone consists of an AB_2 pattern (parameters in Table I).

Figure 13 shows the temperature dependence of the $^{31}P\{^1H\}$ NMR spectrum of $HNi[P(C_2H_5)_3]_3^+B(C_6H_5)_4^-$ in acetone. The calculated spectra were obtained using basic set V (mutual exchange for HML_3^+). An extensive series of line shape simulations were carried out for the $HNiL_3^+$-L system as a function of exchange mechanism, exchange rate, and $[L]/[HML_3^+]$.

Since no resonances other than those assigned to HML_3^+ could be detected at low temperatures, $[L]/[HML_3^+]$ must be small. A small quantity of free ligand could be present in the HML_3^+-acetone solution resulting from either free ligand impurity in the HML_3^+ or from liberation of free ligand from HML_3^+ on dissolution in acetone. The possibility of intermolecular exchange must be considered even in solutions of "pure" HML_3^+.

Figures 14 and 15 show the NMR line shapes calculated for an HML_3^+-L system, using the low temperature (−90°) NMR parameters for $HNi[P(C_2H_5)_3]_3^+$ and $P(C_2H_5)_3$, as a function of exchange rate and exchange mechanism with $[L]/[HML_3^+]$ held constant at 0.00025. Visually indistinguishable results were obtained with $[L]/[HML_3^+]$ set at 0.001. If $[L]/[HML_3^+]$ is raised to 0.01, significantly different line shapes are obtained for all exchange mechanisms except V (mutual exchange). Figure 14 indicates that the basic sets I, II, V, and VII (VII = E + I + II + III + IV + V) give virtually indistinguishable NMR line shapes.

Clearly, no distinction between these basic sets can be made on the basis of the experimental $^{31}P\{^1H\}$ NMR spectra shown in Figure 13. However, analysis of the hydride region ^1H NMR spectra at temperatures below ca. −20° justifies the use of basic set V to fit the $^{31}P\{^1H\}$ spectra (vide infra). Figure 15 indicates that basic sets III and IV would, in practice, be distinguishable for the $HNiL_3^+$-L system using $^{31}P\{^1H\}$ line shape analysis but that the difference is fairly subtle. Since sets III and IV result in a different fast exchange limit to sets I, II, V, and the linear combination VII, they can be distinguished qualitatively. However, it should be noted that linear combinations of III and IV will give a single resonance in the high temperature limit.

The experimental spectra shown in Figure 13 indicate that there are two different exchange processes. As the temperature is raised from the low temperature limit (ca. −90°), the spectrum at first broadens and then coalesces to a single line. These line shape effects are attributed to mutual exchange in the HML_3^+ cation. At still higher temperatures (above ca. −20°), the spectrum broadens again. The nature of the exchange process(es) responsible for the temperature dependence of the NMR line shapes above ca. −20° has not been determined. The exchange rates used to obtain the calculated spectra shown in Figure 13 for the temperatures 11° and −16° were obtained by extrapolation of the rates obtained from the line shape analyses at lower temperatures using the Eyring equation. The temperature dependence of the line shapes is reversible on cycling the temperature in the range −90° to +60°. No irreversible decomposition of HML_3^+ occurs above −20°.

Analysis of the spectra shown in Figure 13 and spectra taken at other temperatures not shown in the figure give the rate of mutual exchange in $HNi[P(C_2H_5)_3]_3^+$ as a function of temperature (thermodynamic parameters in Table III). The small entropy of activation is consistent with a simple intramolecular process.

On adding $P(C_2H_5)_3$ to $HNi[P(C_2H_5)_3]_3^+$ in acetone at −90°, a new resonance, assigned to $HNi[P(C_2H_5)_3]_4^+$, is observed. This resonance is a sharp single line indicating that mutual exchange is rapid in the HML_4^+ cation even at temperatures as low as −90°. The free ligand resonance does not appear in the spectrum until the added ligand concentration exceeds the initial HML_3^+ concentration, indicating that the equilibrium in **8** strongly favors formation of HML_4^+ for M = Ni. Figure 16 shows the temperature dependence of the $^{31}P\{^1H\}$ NMR spectrum for a solution containing 0.18 mol $l.^{-1}$ of $HNi[P(C_2H_5)_3]_3^+B(C_6H_5)_4^-$ and 0.045 mol $l.^{-1}$ of $P(C_2H_5)_3$ in acetone-d_6. The simulations on the right-hand side of the figure were calculated using an HML_4^+-HML_3^+-L model. The slow exchange limit NMR parameters for the AB_3 $^{31}P\{^1H\}$ spectrum of the HML_4^+ species were somewhat arbitrarily set at J_{AB} = 4 Hz, δ_{AB} = 29 Hz (0.8 ppm). The averaged shift is −29.1 ppm upfield from $P(C_2H_5)_3$ at −90°. The mutual exchange rate in the HML_4^+ cation was kept fixed at the high rate of 3×10^5 sec^{-1} since this process is fast even at −90°. Mutual exchange in the HML_3^+ cation was also included, using the exchange rates obtained from the line shape analysis for $HNi[P(C_2H_5)_3]_3^+$ in acetone in the absence of added ligand. However, if this process is omitted from the calculations, the simulated line shapes are not significantly changed since this process is slow relative to the intermolecular process $HML_3^+ + L \rightarrow HML_4^+$ (compare Figures 13 and 16) and the ^{31}P ligand spins are permuted rapidly at the HML_4^+ site. The concentration ratio $[L]/[HML_4^+]$ was kept fixed at 0.001. Calculations, in which $[L]/[HML_4^+]$ was varied, indicate that the line shapes are not sensitive to this ratio provided it is small (0.01 is too large near the slow exchange limit). The observed and calculated spectra shown in Figure 16 are in fairly good agreement at temperatures below ca. −20°. Above this temperature, the spectrum broadens again, as it did for solution with no added ligand. Clearly, the broadening at temperatures above −20° involves species other than $HNiL_4^+$, $HNiL_3^+$, and L. Analysis of the spectra shown in Figure 16 and additional spectra at other temperatures (exchange rates) give the result

$$k_{-1} = 10^{13.3} e^{-10100/RT}$$

for ligand dissociation in $HNiL_4^+$ (Table III). The small positive entropy of activation is consistent with a simple dissociation process. The strong temperature dependence of ligand dissociation in $HNiL_4^+$ supports the assumption that the rate of ligand dissociation in the corresponding Pd and Pt complexes will also be strongly temperature dependent.

For the cases M = Pt, Pd, the equilibrium **8** is strongly to the left-hand side at all accessible temperatures in acetone. Consequently, HML_3^+-L solutions contain very small concentrations of HML_4^+, not readily detected by NMR. Under these circumstances, the second-order rate constant for the reaction $HML_3^+ + L \rightarrow HML_4^+$ can be measured but the rate of ligand dissociation from HML_4^+ cannot. For M = Ni, the equilibrium favors HML_4^+ so that HML_3^+-L solutions contain *either* HML_4^+ and HML_3^+ *or* HML_4^+ and L. Significant concentrations of HML_3^+ and L cannot be obtained simultaneously (this is true for at least the lower part of the temperature range −90° to +60°). Since $[HML_3^+]$ and [L] cannot both be measured, the rate constant for the forward step in **8** cannot be determined. In this case, since $[HML_4^+]$ is large, the rate of ligand dissociation in this five-coordinate cation *can* be determined.

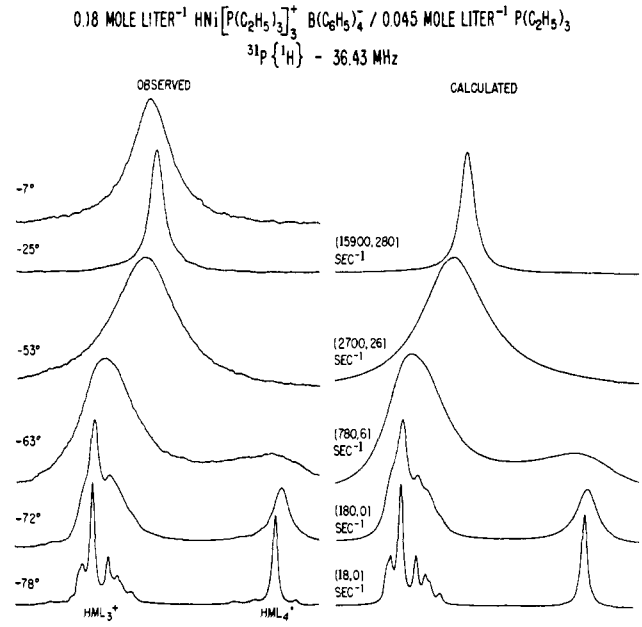

Figure 16. Observed and calculated $^{31}P\{^1H\}$ NMR line shapes for a solution containing 0.18 mol $l.^{-1}$ of $HNi[P(C_2H_5)_3]_3^+B(C_6H_5)_4^-$ and 0.045 mol $l.^{-1}$ of $P(C_2H_5)_3$. The exchange rates are the rate of ligand dissociation from HML_4^+ and the rate of mutual exchange in HML_3^+, respectively.

Experiments similar to that illustrated in Figure 16 were carried out at a variety of added ligand concentrations. If the added ligand concentration is greater than the initial HML_3^+ concentration, the only resonances observable at low temperatures are those assigned to HML_4^+ and L. In this event, the low temperature limit spectrum consists of two singlets and the temperature dependence of the NMR line shapes can be analyzed using a simple two site, one spin model.

Intramolecular rearrangement in the five-coordinate HML_4^+ cation can be slowed down on the NMR time scale at very low temperatures in chlorodifluoromethane. At −157°, the $^{31}P\{^1H\}$ NMR spectrum is an AB_3 pattern with unresolved spin-spin coupling. See Table II for NMR data. As the temperature is raised, the spectrum broadens and coalesces into a single line. Line shape calculations using an AB_3 model indicate that the exchange rate at −147° is about 500 sec^{-1} corresponding to a free energy of activation of ~5.6 kcal mol^{-1}. From this result, we estimate an exchange rate of ~750000 sec^{-1} at −90°, thus, justifying the use of a very large mutual exchange rate for HML_4^+ in analyzing the spectra shown in Figure 16 (and others not shown in the figure) over the temperature range −90° to −20°. These spectra were analyzed before the low temperature experiments had been carried out. Consequently, the correct NMR parameters for HML_4^+ were not used. However, the rate of mutual exchange is so fast for all temperatures in the liquid range of acetone that no significant errors are introduced by using arbitrary NMR parameters for HML_4^+ provided the averaged chemical shift is correct. For this reason, the $HNiL_3^+$-L spectra were not reanalyzed.

B. Hydride Region ^1H Spectra. The temperature dependent hydride region ^1H NMR spectrum for a solution of $HNi[P(C_2H_5)_3]_3^+B(C_6H_5)_4^-$ in acetone-d_6 is shown in Figure 17. As was the case for $HPt[P(C_2H_5)_3]_3^+$ the low temperature limit spectrum cannot be fitted accurately using an AB_2X model, presumably for the same reasons.

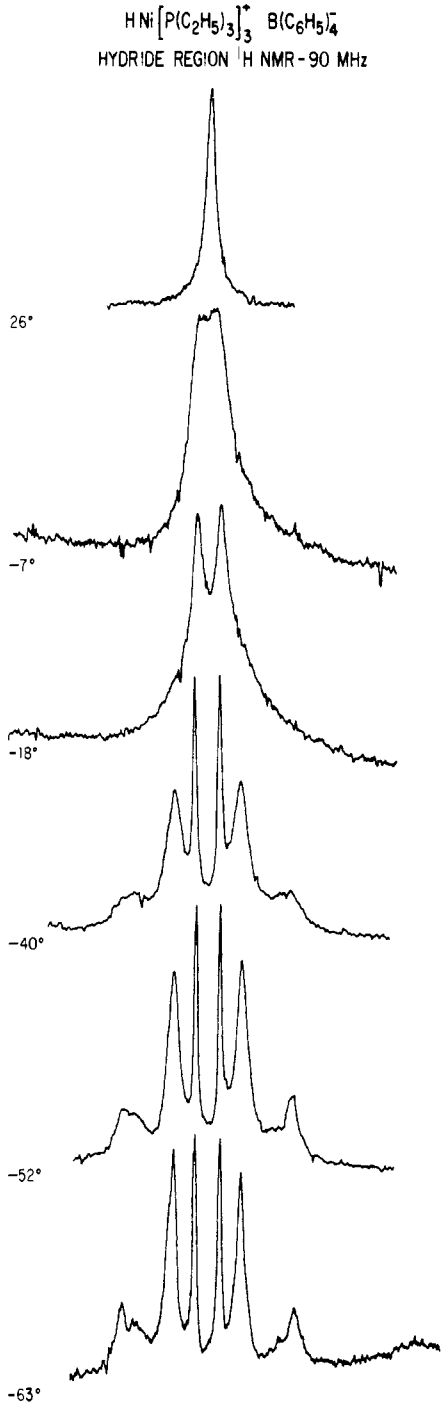

Figure 17. Temperature dependence of the hydride region ^1H NMR spectrum for a solution of $HNi[P(C_2H_5)_3]_3^+B(C_6H_5)_4^-$ in acetone-d_6.

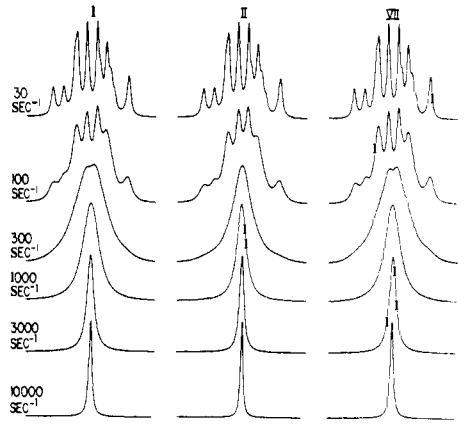

Figure 18. Calculated spectra for the X part of an AB_2X spectrum for the basic sets I and II and the linear combination VII as a function of exchange rate. The slow exchange limit NMR parameters were obtained from analyzing the $^{31}P\{^1H\}$ and ^1H NMR spectra for solutions of $HNi[P(C_2H_5)_3]_3^+B(C_6H_5)_4^-$ in acetone.

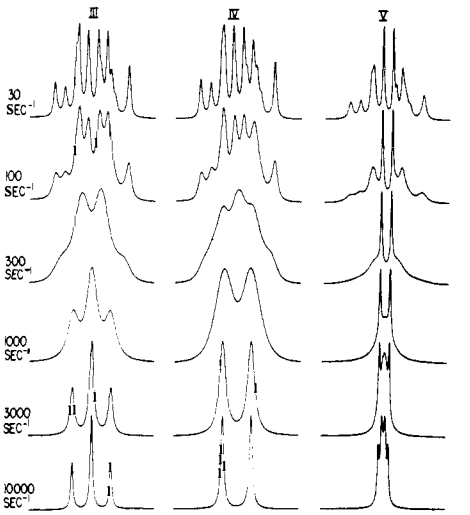

Figure 19. This figure is a continuation of Figure 18 for the basic sets III, IV, and V.

Figures 18 and 19 show NMR line shapes calculated as a function of exchange rate for the basic sets I, II, III, IV, and V and the linear combination VII, using an AB_2X model. Since the ^1H and ^{31}P resonances are not connected by the exchange matrix, the hydride region NMR line shapes are independent of $[L]/[HML_3^+]$ (we are assuming that $[HML_4^+] \rightarrow 0$). Figures 18 and 19 indicate that sets I, II, and VII cannot be readily distinguished using ^1H NMR for M = Ni. Sets III, IV, and V can easily be distinguished from each other and from sets I, II, and VII. Only set V gives line shapes in agreement with those observed experimentally at temperatures in the range −60° to −20° indicating that in this temperature range the line shapes are dominated by mutual exchange in the $HNiL_3^+$ cation. At higher temperatures, a second exchange process causes the spectrum to collapse to a single line instead of the quartet expected for basic set V in the fast exchange limit (Figure 19). Since the slow exchange limit spectra cannot be fitted accurately using an AB_2X model, no attempt was made to carry out a quantitative line shape analysis. Quantitative rate data can be obtained from the $^{31}P\{^1H\}$ spectra (vide supra).

The best agreement between the observed low temperature limit spectrum and calculated spectra using an AB_2X model, with $J_{AB} = 25$ Hz, $\delta_{AB} = 63$ Hz (1.73 ppm), taken from the $^{31}P\{^1H\}$ spectra was obtained using $J_{XA} = \pm 102$ Hz, $J_{XB} = \pm 69$ Hz. These values were used to obtain the calculated spectra shown in Figures 18 and 19.

Figure 20 shows the temperature dependence of the hydride region ^1H NMR for a solution containing approximately 0.175 mol $l.^{-1}$ of $HNi[P(C_2H_5)_3]_3^+B(C_6H_5)_4^-$ and ~0.05 mol $l.^{-1}$ of $P(C_2H_5)_3$. The single resonance at the left-hand side of the figure is assigned to $HNi[P(C_2H_5)_3]_4^+$. The complex pattern on the right-hand side is associated with $HNi[P(C_2H_5)_3]_3^+$. As the temperature is raised, the two sets of resonances broaden and coalesce into a single line indicating exchange between the HML_4^+ and HML_3^+ sites. The reaction $HML_3^+ + L \rightleftharpoons HML_4^+$ is the simplest process which can account for the observed temperature dependence of the spectra shown in

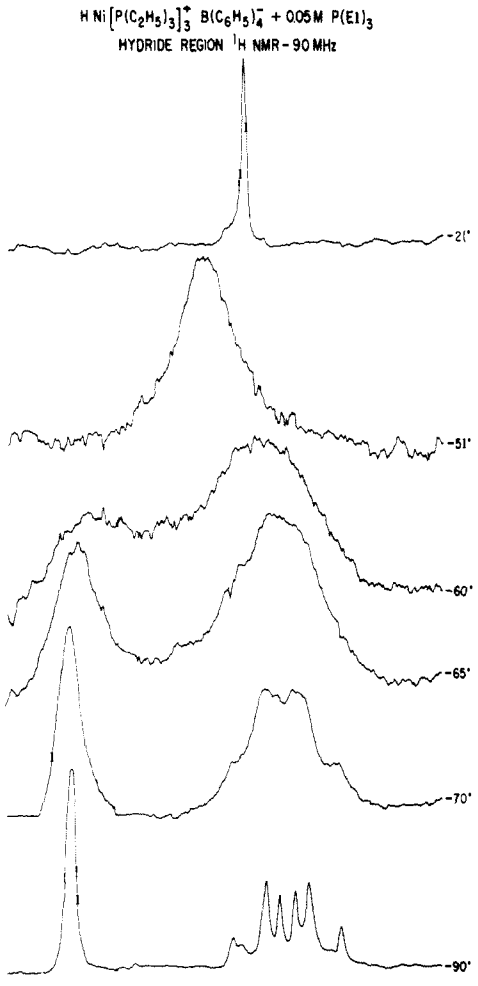

Figure 20. Temperature dependence of the hydride region ^1H NMR spectrum for a solution of 0.175 mol $l.^{-1}$ of $HNi[P(C_2H_5)_3]_3^+B(C_6H_5)_4^-$/0.05 mol $l.^{-1}$ of $P(C_2H_5)_3$ in acetone (i.e., ~0.125 mol $l.^{-1}$ of HML_3^+/~0.05 mol $l.^{-1}$ of HML_4^+).

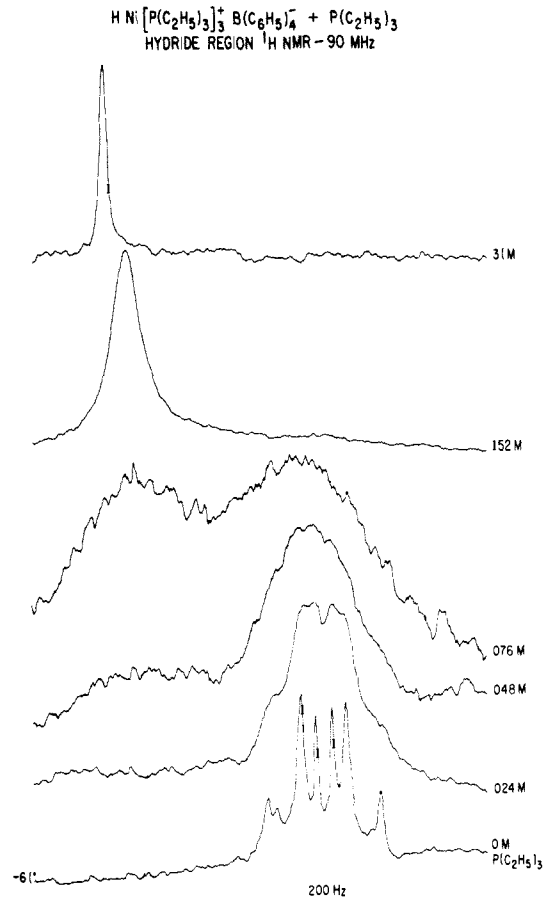

Figure 21. Hydride region ^1H NMR spectra for a solution of $HNi[P(C_2H_5)_3]_3^+B(C_6H_5)_4^-$ as a function of added $P(C_2H_5)_3$ concentration at −61°.

Figure 20. It should be noted that the highest temperature for the spectra shown in Figure 20 is −21°. At these temperatures, the spectra are not complicated by the second unassigned intermolecular exchange process which becomes important only at temperatures above −20°.

Figure 21 shows the hydride region ^1H NMR spectrum for a solution of 0.175 mol $l.^{-1}$ of $HNi[(C_2H_5)_3]_3^+B(C_6H_5)_4^-$ in acetone-d_6 as a function of added ligand concentration. The spectrum on the bottom row corresponds to pure HML_3^+ and that on the top row to a solution containing HML_4^+ and L with a very small HML_3^+ concentration. For added ligand concentrations in the range 0-0.175 mol $l.^{-1}$, both HML_4^+ and HML_3^+ are present in the solution in significant concentrations and line shape effects resulting from their exchange can be seen.

Solvent Effects. Preliminary Consideration

Cations of the type HML_3^+ will be strongly solvated in a polar solvent such as acetone; it is also highly probable that two electron donor solvents such as acetone, acetonitrile, etc.) will enter the inner coordination sphere of the metal to form a five-coordinate 18 electron complex, although the strength of the "bond" to the solvent ligand will usually be weak. For very weak solvent bonding "complexes" in which the strongly attached ligands are still roughly planar with long bonds to the solvent molecule or molecules occupying the apical positions are a possibility (**16**). For a strongly bound solvent molecule, the situation will be similar to attack by a phosphine ligand and a configuration such as **17** is expected. For both **16** and particularly **17**, there is the additional possibility of intramolecular rearrangement after solvent attack.

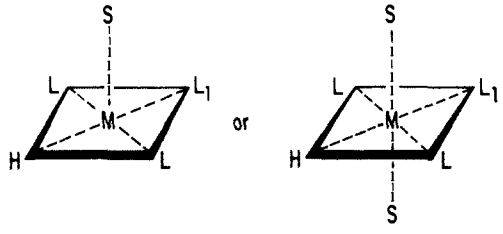

16

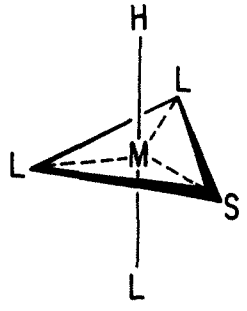

17

We may write the equilibrium as

$$HML_3^+ + xS \underset{k_{-s}}{\overset{k_s}{\rightleftharpoons}} HML_3S_x^+ \qquad (5)$$

for the moment, without inquiring about the stereochemis-

try of $HML_3S_x^+$. k_s and k_{-s} may be extremely rapid reactions, in which case the NMR spectra we have assigned to HML_3^+ will, in fact, correspond to the fast exchange limit for the solvent association reaction.

The direct formation of a complex such as **17** does not appear likely: for the cases of Pd and Pt, the ligand trans to hydride in HML_3^+ retains its unique position (the NMR spectra of $HPdL_3^+$ and $HPtL_3^+$ in acetone are invariant to temperature in the absence of added phosphine) implying that **17** is either rigid on the NMR time scale at high temperatures (an improbable situation) or that it is present in vanishingly small concentrations. The data could be compatible with a configuration such as **16** being a major component in the solution and not being fluxional. It is difficult, however, to distinguish cases such as **16** from nonspecific solvation.

Intermolecular ligand exchange could take place by a process such as

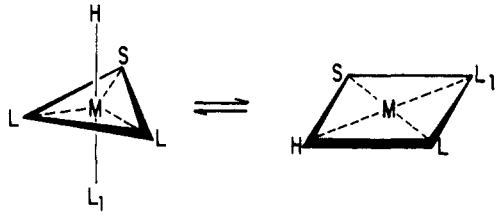

18

However, if this process were important, the intermolecular exchange would proceed without ligand catalysis and the coupling between the hydride proton and the phosphorus nuclei on the two cis ligands would be exchange decoupled even in the absence of added ligand. This exchange decoupling is not observed for M = Pt or for Ni. Since addition of only very small concentrations of free ligand results in rapid intermolecular exchange, the exchange process **18** must be relatively unimportant. For the palladium case, no cis H-P coupling is observed. This could be due to a solvent exchange process but is ruled out by the observation of ^{31}P-^{31}P coupling in the $^{31}P\{^1H\}$ spectrum.

If one wishes to make fine distinctions between specific and bulk solvent effects, species such as **16** could be considered to be the dominant "complexes" in solution. If this is so, ligand catalyzed exchange could take place by (1) addition of free ligand to the small fraction of HML_3^+ in equilibrium with **16** or (2) by displacement of S by free ligand.

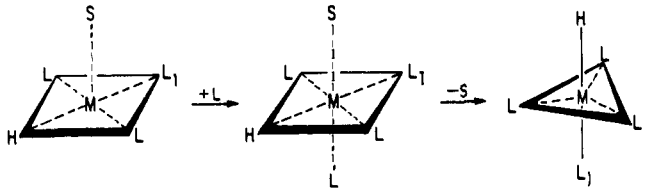

19

19 illustrates a possible solvent displacement sequence. If the M-S bond had significant strength (an unlikely situation since this would almost certainly lead to a fluxional trigonal bipyramidal stereochemistry, which has been ruled out as a major species) the reaction could be regarded as an SN2 displacement. It is probably more realistic to view it as ligand attack on a simple planar species.

In all of the cases discussed above, the rate of the ligand substitution reaction is expected to be solvent dependent. These features will be discussed in more detail in a future publication.

As a final note in this section, a fluxional five-coordinate $HNiL_3S^+$ could provide a mechanism for "mutual exchange" in the $HNiL_3^+$ system.

Discussion

The nuclear resonance data have shown that the HML_3^+ complexes (M = Ni, Pd, Pt; L = $P(C_2H_5)_3$) all have C_{2v} symmetry on the NMR time scale at low temperatures (AB_2 $^{31}P\{^1H\}$; AB_2X ^1H; Table I). The effective C_{2v} symmetry is maintained for the Pd and Pt complexes over the whole temperature range studied (−90° to +60° in acetone). For the Ni complex above ca. −20°, at least two rate processes occur even in the absence of free ligand. The C_{2v} symmetry does not, of course, require a structure in which cis H-M-P and P-M-P bond angles are 90°. Some distortions are anticipated with the two "trans" L ligands being symmetry equivalent. An approximate model for the present compounds could be $HPt[P(C_2H_5)_3]_2Br$ in which the P-Pt-P angle is 172° and the P-Pt-Br angle is 94°,[6] in the solid state, suggesting that the L-L-L steric interactions will reduce the trans P-M-P angle from the idealized 180° and increase the cis P-M-P angle above the idealized 90° in the HML_3^+ species. The question of weak solvent coordination has been discussed briefly in the preceding section.

It has been shown from the mechanistic analysis of the ^1H hydride region NMR of $HNiL_3^+$ that, in the temperature region −63° to −18°, the spectra can be simulated using the permutational set V, and that the mechanism involves a simple intramolecular exchange of the two types of phosphorus ligands (configuration **9**, $\Delta G^\ddagger$ = 11.2 at 200 K, Table III). Tetrahedral stereochemistries are common in the chemistry of four coordinate Ni(II); this would provide an effective pathway for the mutual exchange as shown in configuration **10**. The exchange is *not* ligand catalyzed. Since the ^1H hydride spectrum of HML_3^+ collapses to a single line at 26° (Figure 17) rather than the quartet expected from permutational set V (Figure 19), it is clear that a second, bond breaking process must be important above ~0°C, even in the absence of added ligand. A reaction which is possible, and would be more likely to occur for Ni than Pt or Pd is

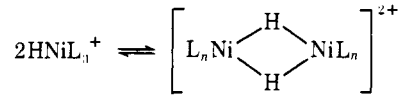

(6)

with n = 2 or 3. A precedent of this is provided by the complexes:

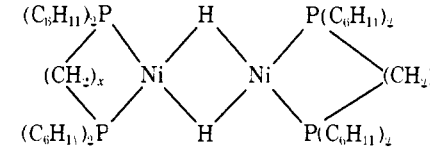

x = 2-4

isolated by Wilke and co-workers, although the oxidation state is different.[7]

Other NMR data (Table II) have shown that addition of excess ligand to HML_3^+ in $CHClF_2$ solution at low temperatures ca. −150° leads to intermediates of the form HML_4^+ which have C_{3v} symmetry on the NMR line scale (AB_3 $^{31}P\{^1H\}$ NMR spectra). The structures presumably lie between idealized trigonal bipyramids and regular tetrahedral arrays of phosphorus ligands with the hydride ligand in the center of a tetrahedral face. An example of a structure of the latter type is found for $HRh[P(C_6H_5)_3]_4$ where the phosphorus atoms lie at the corners of a regular tetrahedron.[8] Stable HML_4^+ molecules have been studied in detail using NMR line shape methods;[9] in general they have very low barriers to intramolecular rearrangement. The two most likely idealized mechanisms for intramolecular exchange in simple five-coordinate transition metal complexes

are the Berry process[10] and the tetrahedral jump,[9] corresponding to the two limiting idealized ground state stereochemistries. In the present study only the $HNiL_4^+$ intermediate is sufficiently stable (present in sufficiently high concentrations) to allow a determination of the free energy of activation for intramolecular rearrangement ($\Delta G^\ddagger$ = 5.6 kcal mol^{-1} at 126 K, Table III).

For all three metals, addition of free L to HML_3^+ results in nuclear resonance line shape effects which are interpreted in terms of the ligand catalyzed exchange:

$$HML_3^+ + L \underset{k_{-1}}{\overset{k_1}{\rightleftharpoons}} HML_4^+ \qquad (7)$$

The reaction is further supported by the fact that all three species in the equation can be detected for all three metals under suitable conditions.

The following detailed conclusions with regard to eq 7 can be reached, based on the results presented earlier in the paper.

(a) For M = Pt the kinetics correspond to an expression of the form

$$1/\tau_{HPtL_3^+} \propto [L]^{1.0}[HPtL_3^+]^0$$

with the activation parameters given in Table III. The concentration dependences and large negative entropy of activation are in accord with an associative mechanism.

The equilibrium constant is expected to be strongly temperature dependent since a weak temperature dependence has been shown for k_1 experimentally and a strong temperature dependence is expected for k_{-1} ($\Delta H^\ddagger$ is anticipated to be nonzero and $\Delta S^\ddagger \sim 0$ for a simple dissociative step). This means that $[HPtL_4^+]$ decreases rapidly with temperature, allowing calculations to be carried out in the −90° to +30° range which assume a very small concentration and preexchange lifetime for $[HPtL_4^+]$. This approach has also been justified theoretically.[2]

With the above information, the nuclear resonance line shape calculations shown in Figures 1, 2, and 4 could be carried out. The calculated line shapes correspond to basic set IV (E + IV), the only set which gives agreement with experiment. *The results constitute direct evidence for ligand attack along the pseudo C_4 axis of the planar $HPtL_3^+$ species, leaving the ligand trans to hydride unique, with the attacking ligand ending in a position symmetry equivalent with the positions of the two trans phosphorus ligands* (i.e., off the C_3 axis of the C_{3v} five-coordinate intermediate). The five-coordinate intermediate has a very short life and, on the average, it does not have time to undergo mutual exchange before dissociation. Dissociation must occur from an equatorial position by microscopic reversibility.

Hence for the Pt system

$$k_{-1} \gg k_m \text{ (both very fast)}$$

$$k_m' \text{ is slow}$$

$$k_1(T) = 10^{7.07}e^{-3030/RT} \text{ l. mol}^{-1} \text{ sec}^{-1}$$

(b) For M = Pd the general considerations are similar to those for Pt. The major difference is that the intramolecular rearrangement in $HPdL_4^+$, although still slower than ligand dissociation, is fast enough to have observable effects on the NMR spectra and the two competing processes must be included explicitly in the calculations. Instead of the combination of basic sets (E + IV) used for Pt, the combination[2] $(1 - C)(E + IV) + (C/3)(I + II + III + V)$ must be used where C is related to k_m/k_{-1}. Ratios of k_m/k_{-1} as a function of temperature can be obtained from the line shape calculations (Table IV).

The small temperature dependence of k_m/k_{-1} implies similar Arrhenius activation parameters; k_{-1} is approximately two orders of magnitude faster than k_m at all temperatures in the range −90° to +60°.

Hence for the Pd system

$$k_{-1} \approx 10^2 k_m \text{ (both very fast)}$$

$$k_m' \text{ is slow}$$

$$k_1(T) = 10^{7.07}e^{-2400/RT}$$

(c) For M = Ni again the general considerations are the same, with the following modifications: (1) the intramolecular rearrangement in $HNiL_3^+$ proceeds at a measurable rate; (2) the equilibrium (7) lies well to the right; (3) since appreciable concentrations of $HNiL_4^+$ are present, the intramolecular rearrangement in this complex can be studied quantitatively; (4) k_{-1} can be determined directly (k_1 cannot).

The strong temperature dependence of k_{-1} supports the assumption that k_{-1} is strongly temperature dependent for the Pt and Pd systems.

In summary for the Ni complexes

$$k_{-1}(T) = 10^{13.3}e^{10100/RT}$$

$$k_m(T) = \frac{kT}{h}e^{-5600/RT} \text{ (assuming } \Delta S^\ddagger \text{ is small)}$$

$$k_m'(T) = 10^{11.3}e^{-10000/RT}$$

Conclusion

A rather complete picture has been developed for the rate processes occurring in solutions of HML_3^+ complexes with and without excess ligand. General computer programs applicable to intermolecular exchange in non-first-order spin systems have been utilized in interpreting the NMR data. Four separate rate processes have been considered, k_1, k_{-1}, k_m (the rate of intramolecular rearrangement in HML_4^+), and k_m' (the rate of intramolecular rearrangement in HML_3^+).

Permutational analyses have been carried out for the combined inter-intramolecular case, which are an extension of those we have developed earlier for intramolecular rearrangements. The approach allows one to extract detailed mechanistic information concerning the mode of ligand attack and the site occupied by the attacking ligand in the five-coordinate intermediate. The mechanistic data and much of the quantitative kinetic data would be difficult to obtain using other approaches, particularly since the entering and leaving ligands are identical. A schematic representation of the overall reaction system is shown in Figure 22.

The study provides, for the first time, a quantitative determination of rates of ligand exchange vs. intramolecular rearrangement in the association reactions of planar d^8 transition metal complexes. In this paper we have concentrated on ligand catalyzed steps; the role of the solvent will be explored in future work.

Quantitative NMR line shapes studies of ligand substitution processes coupled with group theoretical analyses of mechanistic pathways are a valuable approach in the investigation of kinetics and mechanisms of organometallic reactions. The results of this study and other recent NMR studies[11] have provided a more detailed insight into planar substitution reactions than was previously possible; future studies will be aimed at the role of solvent, reactions in which the attacking group differs from the leaving group, trans labilization (it is interesting to note that in the present study it is *not* the ligand trans to H which is involved in the exchange process), and isomerization processes. It seems like-

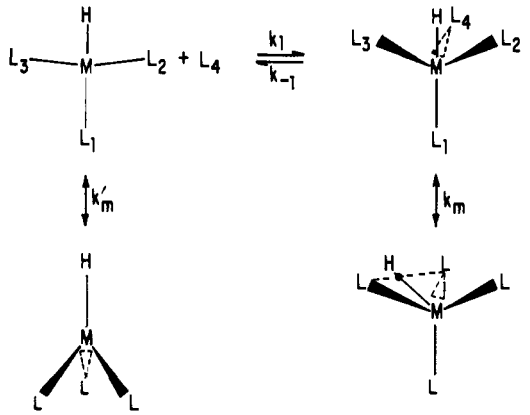

Figure 22. Schematic representation of overall reaction system. The k_m process is shown as going by the "tetrahedral jump" mechanism as opposed to the Berry mechanism since the HML_4^+ cation is expected to be distorted in the manner shown ($P(C_2H_5)_3$ is a bulky ligand). The k_m and k_{-1} processes are expected to be relatively insensitive to solvent. The k_m' and particularly the k_1 process are expected to show significant solvent effects due to weak inner sphere solvation.

ly that most of the phenomena can be encompassed mechanistically in sequences of four coordinate "planar" association, five-coordinate "trigonal bipyramidal" dissociation reactions, with competing intramolecular rearrangement in the five-coordinate complexes. In some cases, a solvent molecule may occupy one of the sites in the five-coordinate species. Many of the species could be present in very small concentrations and would escape detection in most classical approaches to planar substitution. The intermediate $HPtL_4^+$, clearly identified in the present work, is a case in point.

Acknowledgment. We would like to thank Mr. M. A. Cushing for preparation of some of the complexes and Messrs. G. Watunya and F. N. Schock for obtaining many of the NMR spectra.

References and Notes

(1) P. Meakin, R. A. Schunn, and J. P. Jesson, *J. Am. Chem. Soc.*, **96**, 277 (1974).
(2) P. Meakin, A. D. English, and J. P. Jesson, *J. Am. Chem. Soc.*, preceding paper in this issue.
(3) R. A. Schunn, to be submitted for publication.
(4) The least-squares analysis was carried out using the program ARH2 supplied by Professor J. D. Roberts.
(5) T. W. Dingle and K. R. Dixon, *Inorg. Chem.*, **13**, 846 (1974).
(6) P. G. Owston, J. M. Partridge, and J. M. Rowe, *Acta Crystallogr.*, **13**, 246 (1960).
(7) K. Jonas and G. Wilke, *Angew. Chem., Int. Ed. Engl.*, **9**, 312 (1970).
(8) R. W. Baker and P. Pauling, *Chem. Commun.*, 1495 (1969).
(9) P. Meakin, E. L. Muettertles, and J. P. Jesson, *J. Am. Chem. Soc.*, **94**, 5271 (1972).
(10) R. S. Berry, *J. Chem. Phys.*, **32**, 933 (1960).
(11) P. Meakin, A. D. English, and J. P. Jesson, *J. Am. Chem. Soc.*, submitted for publication.

Site of Nucleophilic Attack on Acylpentacarbonylmanganese(I) Compounds

Charles P. Casey* and Charles A. Bunnell

Contribution from the Department of Chemistry, University of Wisconsin, Madison, Wisconsin 53706. *Received April 28, 1975*

Abstract: Methyllithium reacts with benzoylpentacarbonylmanganese(I) at a coordinated CO to give lithium *cis*-acetylbenzoyltetracarbonylmangan(I)ate (**1b**) which was isolated as the tetramethylammonium salt **1a**. **1a** was characterized by ir, NMR, and x-ray crystallography. **1a** decomposes to acetophenone via preferential phenyl migration to manganese as determined by ^{13}C labeling studies.

Nucleophilic attack upon a carbon atom coordinated to a transition metal is an important process in the preparation of new organometallic complexes and in the generation of reactive intermediates useful for organic synthesis. While there is some information available concerning the relative reactivity of various ligands towards nucleophiles, it is not now possible to predict the site of nucleophilic attack in a polyfunctional organometallic compound.

In the case of simple metal carbonyls, attack of organolithium reagents at a coordinated CO group is well known. The first synthesis of a stable transition metal carbene complex utilized the reaction of C_6H_5Li with $W(CO)_6$ to give an isolable acylpentacarbonyltungsten anion which was subsequently alkylated on oxygen to give $(CO)_5WC(OCH_3)C_6H_5$.[1] Reaction of organolithium reagents with $Fe(CO)_5$ led to acyl tetracarbonylferrates[2] which have proven to be extremely useful reagents for the synthesis of organic carbonyl compounds.[3] In the case of $LM(CO)_5$ where two sites of attack are possible, nucleophilic attack of $C_6H_5CH_2MgCl$[4] and CH_3Li[5] on $LM(CO)_5$ gives cis acyl anions.

For transition metal carbene complexes such as $(CO)_5WC(OCH_3)C_6H_5$, nucleophilic attack could in principle occur at either a coordinated CO or at the carbene carbon atom. However, only reaction at the carbene carbon atom is observed.[6] Reaction of amines and thiols with alkoxy substituted carbene complexes proceeds by attack at the carbene carbon atom and leads to amino and thiol substituted carbene complexes.[7,8] Stable addition products have been isolated in the case of diazabicyclo[2.2.2]octane[9] and trimethylphosphine.[10] While attack of amines at CO might be fast and reversible in these cases, the kinetically preferred site must also be the carbene carbon atom since C_6H_5Li reacts with $(CO)_5WC(OCH_3)C_6H_5$ at the carbene carbon atom to give an adduct which can be converted to $(CO)_5WC(C_6H_5)_2$ on treatment with HCl.[11]

The similarity between the structure of acyl metal compounds and of alkoxy carbene complexes makes a comparison of their relative reactivity interesting. Transesterifica-